Experimental Cell Research 460 (2026) 115070

Contents lists available at ScienceDirect

Experimental Cell Research

journal homepage: www.elsevier.com/locate/yexcr

Research article

A novel chalcone analog inhibits cancer stemness in CD44$^+$ and CD133$^+$ populations via suppression of ERK signaling

Suji Baek [a,1], Seojin Jang [b,1], Sei Young Lee [c,1], Seo Lyn Choi [d,e], Jeong-Yoon Yang [e,f], Jung Ho Park [f,g], Bom Sahn Kim [h], Seok-Hyung Kim [i], Jae Jun Lee [j], Sang-Hyuk Lee [d,e], Byung Seok Moon [h,*], Chang-Whan Yoon [d,e,**], Kang Pa Lee [a,***]

[a] Research and Development Center, UMUST R&D Corporation, Seoul, 01413, South Korea
[b] Department of Health Sciences and Technology, Samsung Advanced Institute for Health Sciences & Technology, Sungkyunkwan University, Seoul, 06355, South Korea
[c] Department of Otorhinolaryngology-Head and Neck Surgery, Chung-Ang University Hospital, Chung-Ang University College of Medicine, Seoul, 06973, South Korea
[d] Department of Otorhinolaryngology-Head and Neck Surgery, Sungkyunkwan University School of Medicine, Kangbuk Samsung Hospital, Seoul, 03181, South Korea
[e] Medical Research Institute, Kangbuk Samsung Hospital, Sungkyunkwan University School of Medicine, Seoul, 03181, South Korea
[f] Endocura Inc., Medical Research Institute, Kangbuk Samsung Hospital, Seoul, 03181, South Korea
[g] Department of Internal Medicine, Kangbuk Samsung Hospital, Sungkyunkwan University College of Medicine, Seoul, 03181, South Korea
[h] Department of Nuclear Medicine, Ewha Womans University College of Medicine, Seoul, 07804, South Korea
[i] Department of Pathology, Samsung Medical Center, Sungkyunkwan University School of Medicine, Seoul, 06351, South Korea
[j] Non-Clinical Evaluation Center, OSONG Medical Innovation Foundation (K-BIO), Chengju-si, Chungbuk, 361-951, South Korea

ARTICLE INFO

Keywords:
Chalcone
CD44
CD133
Cancer stem-like cell
Organoid

ABSTRACT

Cancer stem-like cells (CSC) that express cluster of differentiation (CD)44 or CD133 contribute to tumor aggressiveness, therapeutic resistance, and disease recurrence across multiple malignancies. Consequently, current therapeutic modalities frequently fail to achieve durable disease control; hence, novel therapeutic strategies are urgently required. Therapeutic strategies that disrupt CSC maintenance may therefore contribute to more durable cancer control. Suitably, chalcone-based analogs have emerged as promising anticancer candidates. Therefore, this study aimed to investigate the effects of a novel chalcone analog 1 (UR-1) on CSC populations characterized by CD44$^+$ or CD133$^+$ phenotypes using complementary three-dimensional culture systems and *in vivo* models. CD44$^+$ or CD133$^+$ CSC populations were enriched from human head and neck squamous cell carcinoma, gastric cancer, breast cancer, lung cancer, colorectal cancer, and hepatocellular carcinoma cell lines. The effects of the novel chalcone-based 1 (UR-1) on CSC-associated phenotypes were evaluated *in vitro* and in organoid-derived xenograft models. Stemness-associated markers and apoptotic signaling were assessed via immunoblotting and immunofluorescence analyses. Structure-based analyses revealed that UR-1 favorably interacts with surface-accessible binding pockets of both CD44 and CD133, with comparable binding affinity toward the two CSC markers. Mechanistically, UR-1 markedly suppressed ERK phosphorylation (p-ERK), thereby attenuating downstream signaling associated with CSC maintenance. Consistent with these findings, UR-1 markedly suppressed the expression of stemness-associated proteins and impaired spheroid- and organoid-forming capacity in CD44$^+$ cancer cells derived from multiple tumor types. Similar inhibitory effects were observed in CD133$^+$ CSC populations derived from lung, colorectal, and liver cancers, where UR-1 reduced three-dimensional growth and stemness marker expression. In CD133$^+$ cancer organoid models, UR-1 disrupted organoid architecture and decreased the expression of CD133 and SOX2. Furthermore, UR-1 treatment markedly attenuated stemness marker expression and induced cleaved caspase-3-positive apoptotic signaling in CD44$^+$ or CD133$^+$ organoid-derived xenografts.

These findings demonstrate that UR-1 suppresses stemness and promotes apoptosis in CD44$^+$ and CD133$^+$ CSC populations in association with suppression of ERK phosphorylation. By targeting this critical signaling axis, UR-

* Corresponding author.
** Corresponding author. Department of Otorhinolaryngology-Head and Neck Surgery, Sungkyunkwan University School of Medicine, Kangbuk Samsung Hospital, Seoul 03181, South Korea
*** Corresponding author.
E-mail addresses: bsmoon@ewha.ac.kr (B.S. Moon), researchy2024@nate.com (C.-W. Yoon), umustrnd@naver.com (K.P. Lee).
[1] These authors contributed equally to this work.

https://doi.org/10.1016/j.yexcr.2026.115070
Received 13 February 2026; Received in revised form 13 May 2026; Accepted 14 May 2026
Available online 15 May 2026
0014-4827/© 2026 The Authors. Published by Elsevier Inc. This is an open access article under the CC BY license (http://creativecommons.org/licenses/by/4.0/).

1 attenuates CSC-driven tumor progression and therapeutic resistance, highlighting its potential as a promising therapeutic candidate.

1. Introduction

The effective treatment of aggressive malignancies remains a major clinical challenge in modern oncology. Specifically, current therapeutic modalities frequently fail to achieve durable disease control [1,2]. Although advances in chemotherapy, targeted therapy, and immunotherapy have improved initial treatment responses and prolonged patient survival in certain cancer types, disease relapse and acquired therapeutic resistance remain pervasive obstacles [3,4]. Correspondingly, tumor recurrence following an initial therapeutic response is often associated with increased aggressiveness, enhanced metastatic potential, and diminished responsiveness to subsequent treatments. This ultimately leads to poor clinical outcomes [3,5].

Cancer stem-like cells (CSC) are a distinct subpopulation of tumor cells characterized by self-renewal capacity, multilineage differentiation potential, and pronounced resistance to conventional chemo- and radiotherapy [6–8]. Moreover, CSCs play an essential role in tumor relapse and therapy resistance across diverse malignancies [9–12]. CSCs constitute a small but highly aggressive subpopulation within tumors that is endowed with self-renewal capacity, multilineage differentiation potential, and remarkable adaptability to therapeutic stress [12–14]. Unlike the bulk of tumor cells, CSCs can survive conventional cytotoxic treatments and subsequently drive tumor regrowth, metastatic dissemination, and long-term disease persistence [10,11,15]. CSC populations have consistently demonstrated residual enrichment following chemotherapy or radiotherapy, thereby implicating CSC survival as a critical determinant of treatment failure and disease recurrence [6–8,12,16].

Among CSC populations, cells characterized by the expression of cluster of differentiation (CD)44 or CD133 exhibit intrinsic resistance mechanisms, including enhanced DNA damage repair, activation of anti-apoptotic signaling pathways, metabolic reprogramming, and efficient reactive oxygen species scavenging [17–20]. These properties enable $CD44^+$ or $CD133^+$ CSCs to survive therapeutic insults that effectively eliminate differentiated tumor cells. Hence, these CSCs serve as cellular reservoirs for tumor regrowth.

Importantly, resistance mediated by $CD44^+$ or $CD133^+$ CSC populations is not restricted to a single treatment modality but extends across chemotherapy, targeted therapy, and immunotherapy [12, 17, 21]. This highlights their role as a central obstacle to durable cancer control. Consequently, therapeutic strategies that fail to eradicate $CD44^+$ or $CD133^+$ CSCs often result in transient tumor regression followed by inevitable relapse. This reinforces the rationale for directly targeting these CSC populations as an essential component of effective anticancer therapy [9,19,21–23].

Suitably, chalcone-based analogs have emerged as promising anticancer candidates owing to their α,β-unsaturated carbonyl scaffold, structural simplicity, and high chemical tunability [24–26]. These properties enable chalcone derivatives to modulate diverse oncogenic signaling pathways involved in cell proliferation, survival, apoptosis, and stress adaptation, rendering them attractive platforms for anticancer drug development [27–29].

Considering the limitations of current therapeutic modalities, novel therapeutic strategies capable of achieving sustained tumor suppression and preventing disease recurrence [30,31] are urgently needed. Notably, certain chalcone derivatives interfere with stemness-associated signaling networks; hence, these compounds may be effective against therapy-resistant CSC populations [32–34].

Therefore, this study aimed to investigate the potential of a chalcone analog (UR-1) to target $CD44^+$ and $CD133^+$ CSC populations. UR-1 was designed by structurally transforming a salicylic acid-inspired framework into a chalcone scaffold. UR-1 was selected for further evaluation based on its predicted interaction with CD44/CD133 and its structurally favorable chalcone scaffold. This design broadened the modulation of inflammatory, stress-responsive, and survival-associated signaling pathways implicated in CSC maintenance, survival, and phenotypic plasticity. In particular, this study hypothesized that this structural design would interfere with stemness maintenance programs, rather than merely suppressing downstream inflammatory mediators.

Accordingly, UR-1 was systematically evaluated using CSC-enriched spheroid, organoid, and organoid-derived xenograft models across multiple cancer types. Through this integrative experimental framework, this study ultimately aimed to determine whether UR-1 could overcome the key limitations of current anticancer therapies by suppressing stemness-associated phenotypes and impairing the survival of highly tumorigenic treatment-resistant cell populations.

2. Materials and methods

2.1. Cell lines and reagents

Human lung adenocarcinoma (A549), colorectal cancer (SW480), hepatocellular carcinoma (HepG2), head and neck squamous cell carcinoma (SCC-15), gastric cancer (N87), and breast cancer (MDA-MB-231) cells were obtained from the American Type Culture Collection (Manassas, VA, USA). A549, SW480, HepG2, and MDA-MB-231 cells were maintained in Dulbecco's Modified Eagle Medium (DMEM), whereas SCC-15 cells were cultured in DMEM with Ham's F-12 Nutrient Mixture (DMEM/F12) and N87 cells in Roswell Park Memorial Institute (RPMI)-1640. All media were supplemented with 10% fetal bovine serum and 1% penicillin-streptomycin. Cells were cultured at 37 °C in a humidified incubator with 5% CO_2.

2.2. Chalcone analog synthesis

A novel chalcone analog 1 (UR-1, (E)-5-(2-(2-(3-(2,3-dimethoxyphenyl)acryloyl)-4-methoxyphenoxy)acetamido)-2-hydroxybenzoic acid) was synthesized through a two-step reaction sequence as outlined in Fig. 1A. First, 5-aminosalicylic acid (**2**) was reacted with chloroacetyl chloride in the presence of triethylamine as a base in dichloromethane. This reaction afforded the corresponding chloroacetamide intermediate (**3**) via acylation of the amino group. The resulting chloroacetamide intermediate (**3**) was subjected to a nucleophilic substitution reaction with a 2′-hydroxy-2, 3, 5′-trimethoxychalcone (**2**, DK-143) bearing phenolic hydroxyl groups. The coupling reaction was carried out in the presence of potassium carbonate as a base, thereby facilitating O-alkylation through displacement of the chloride group.

The final chalcone analog 1 (UR-1), in which the salicylic acid-derived moiety is covalently linked to the chalcone scaffold via an ether linkage, was obtained at a yield of 5.3%. The structure of the synthesized 1 was confirmed via spectroscopic analyses: ^{1}H NMR (400 MHz, DMSO-d_6) δ 11.15 (brs, 1H), 10.15 (s, 1H), 8.16 (d, J = 2.8 Hz, 1H), 7.77 (dd, J = 40, 16 Hz, 2H), 7.63 (t, J = 4.4 Hz, 1H), 7.44 (d, J = 6.8 Hz, 1H), 7.16 (s, 3H), 7.08 (d, J = 7.2 Hz, 1H), 7.00 (d, J = 8.0 Hz, 1H), 6.91 (d, J = 9.2 Hz, 1H), 4.80 (s, 2H), 3.81 (s, 3H), 3.77 (s, 3H), 3.75 (s, 3H); ^{13}C NMR (100 MHz, DMSO-d_6) δ 187.8, 172.6, 168.1, 164.5, 151.48, 151.42, 150.3, 148.3, 141.0, 133.7, 128.8, 128.2, 122.0, 121.9, 121.38, 124.34, 121.1, 120.8, 118.6, 117.1, 115.8, 114.5, 105.9, 66.6, 61.7, 56.1, 55.8; MS (ESI) m/z 508 (MH^+).

2.3. Structure-based molecular docking

The chemical structure of UR-1 was generated using ChemDraw

v20.0. Three-dimensional structures of CD44 and CD133 were obtained from the Protein Data Bank or generated by homology modeling using SWISS-MODEL [35]. Protein preparation was performed using AutoDock Tools v1.5.7 [36]. Molecular docking simulations were conducted with AutoDock Vina v1.2.3 [37], and docking poses were visualized using PyMOL v2.5.4 [38]. Relative binding affinity was estimated based on docking scores.

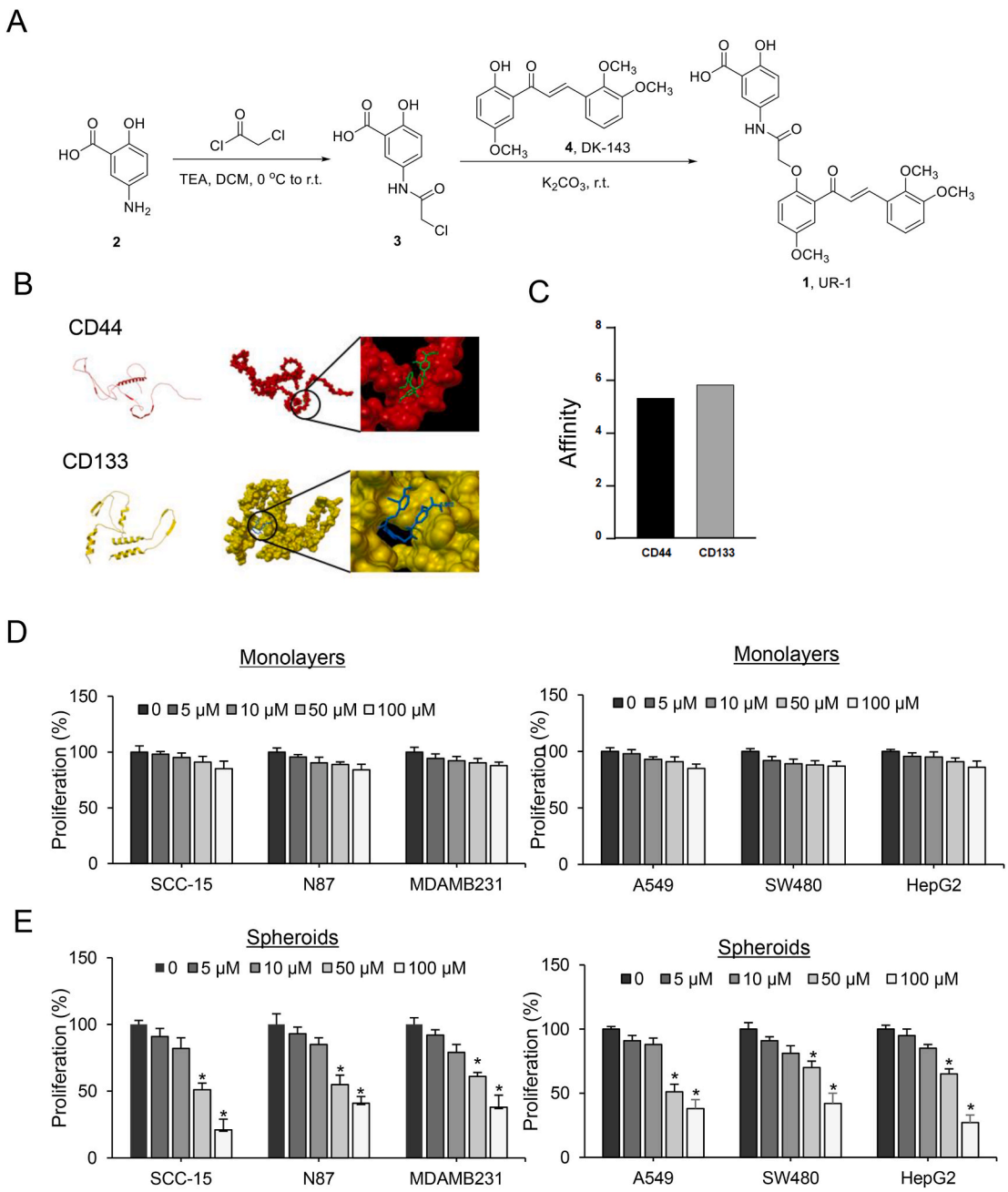


Fig. 1. Structure-based molecular docking and functional validation of UR-1 targeting CD44$^+$ and CD133$^+$ cancer stem-like cells. (A) Schematic representation of the structural design and chemical construction of the UR-1 compound. The workflow illustrates the stepwise assembly of the UR-1 molecular structure, highlighting key chemical moieties and structural features incorporated during the design process. The final chemical structure of UR-1 is shown, suggesting the functional groups relevant to its biological activity. (B) Predicted three-dimensional structures of CD44 (upper panel, red) and CD133 (lower panel, yellow) are shown with docked UR-1 molecules. Magnified views highlight the ligand-binding pockets, with stable accommodation of UR-1 within surface-accessible cavities of both proteins. UR-1 is depicted in stick representation within the binding interface. (C) Comparative docking scores of UR-1 toward CD44 and CD133, which demonstrate favorable and comparable binding affinity to both cancer stem cell markers. (D) Quantitative analysis of cell proliferation in CD44$^+$ and CD133$^+$ cancer cells treated with increasing concentrations of UR-1. UR-1 treatment resulted in a dose-dependent decrease in proliferation, with a more pronounced inhibitory effect observed in CSC-enriched populations. (E) Functional assessment of spheroid formation under UR-1 treatment. Quantitative analysis demonstrates reduced spheroid formation efficiency in CD44$^+$ and CD133$^+$ cells, supported by representative bright-field images showing decreased spheroid size and loss of compact structure following UR-1 exposure.

Data are presented as mean ± standard deviation (SD) from three independent biological replicates (n = 3). Statistical significance was determined using Student's t-test for comparisons between two groups or one-way ANOVA followed by Tukey's post hoc test for multiple comparisons. P values are indicated as $P < 0.05$. (For interpretation of the references to color in this figure legend, the reader is referred to the Web version of this article.)

2.4. Cell growth and proliferation assays

For cell growth analysis, UR-1-treated cells were seeded at a density of 1×10^3 cells/well in 24-well plates. Cells were harvested at the indicated time points (0–8 days) and counted using the trypan blue exclusion method. Cell growth curves were generated based on viable cell counts.

For the cell proliferation assay, cells were seeded at a density of 1×10^3 cells/well in 24-well plates. After incubation for 24, 48, or 72 h, water-soluble tetrazolium 8 (WST-8) reagent (Cat. No. WQ3000, WST-8 Cell Viability Assay Kit) was added to each well according to the manufacturer's instructions. Absorbance was measured at 450 nm using a microplate reader and proliferation was quantified accordingly.

2.5. Gene knockdown and CRISPR activation

Stable knockdown of CD44 and CD133 was achieved using short hairpin RNA (shRNA) constructs (sc-400209-KO-2 and sc-418,263, Santa Cruz Biotechnology). A scrambled shRNA construct (sh.Scr) was used as a negative control. For gene upregulation, CD44 and CD133 expression was induced using CRISPR activation (CRISPRa) plasmids (sc-400209-ACT and sc-418263-ACT, Santa Cruz Biotechnology). A matched non-targeting CRISPRa control plasmid (sc-437,281, Santa Cruz Biotechnology) was used as a negative control. Cells were transduced or transfected with the indicated shRNA constructs or CRISPRa plasmids according to the manufacturer's instructions, followed by puromycin selection to establish stable cell lines. The efficiency of CD44 and CD133 knockdown or upregulation was confirmed by Western blot analysis.

2.6. Spheroid formation assay

For spheroid formation assays, cells were seeded at a density of 1×10^4 cells/well in low-attachment plates containing spheroid culture medium and maintained for 3–5 days. The spheroid culture medium consisted of Advanced DMEM/F12, supplemented with B27 (1×; Cat. No. 17504044, Gibco, Thermo Fisher Scientific, Waltham, MA, USA), N2 (1×, Cat. No. 17502048, Gibco), epidermal growth factor (EGF, 10 ng/mL; Cat. No. 17502048, Gibco), and basic fibroblast growth factor (bFGF, 10 ng/mL; Cat. No. GF003AF, Sigma-Aldrich, St. Louis, MO, USA).

2.7. Magnetic cell sorting

$CD44^+$ or $CD133^+$ spheroid populations were isolated from dissociated tumor spheroids using anti-CD44 MicroBeads (Cat. No.130-095-194, Miltenyi Biotec, Bergisch Gladbach, Germany) or anti-CD133 MicroBeads (Cat. No. 130-097-049, Miltenyi Biotec), respectively, according to the manufacturer's instructions. Briefly, tumor spheroids were enzymatically dissociated into single-cell suspensions using Accutase (Cat. No. A1110501; Life Technologies, Thermo Fisher Scientific) and incubated with anti-CD44 or anti-CD133 magnetic beads at 4 °C for 15 min. The labeled cells were subsequently passed through MS columns placed in a magnetic field (Cat. No. 130-042-201, Miltenyi Biotec), and $CD44^+$ or $CD133^+$ cells were collected from the column. The purity of the isolated cell population was assessed via flow cytometry using fluorophore-conjugated anti-CD44 antibody or anti-CD133 antibodies. Only samples with a purity greater than 90% $CD44^+$ or $CD133^+$ cells were used for downstream experiments.

2.8. Organoid formation assay

For organoid formation [39,40], $CD44^+$ or $CD133^+$ spheroids were isolated using magnetic-activated cell sorting (Miltenyi Biotec) and embedded in Matrigel (Cat. No. 356255, BD Biosciences, Franklin Lakes, NJ, USA), followed by overlay with organoid culture medium in 24-well plates. The organoid medium consisted of the following: DMEM/F12 supplemented with penicillin-streptomycin, 10 mmol/L HEPES, GlutaMAX, B27, N2, N-acetylcysteine (1.25 mmol/L; Cat. No. A9165, Sigma-Aldrich), EGF (0.05 mg/mL; Cat. No. 9644, Sigma-Aldrich), bFGF (0.1 mg/mL; Cat. No. GF003AF, Sigma-Aldrich), gastrin I (0.01 mmol/L; Cat. No. G9145, Sigma-Aldrich), nicotinamide (10 mmol/L; Cat. No. N0636, Sigma-Aldrich), Y-27632 (10 mmol/L; Cat. No. Y0503, Sigma-Aldrich), and SB202190 (Cat. No. S7067, Sigma-Aldrich); Prostaglandin E2 (1 mmol/L; Cat. No. 2296, Tocris Bioscience, Bristol, UK); fibroblast growth factor-10 (0.1 mg/mL; Cat. No. 100-26, PeproTech, Cranbury, NJ, USA); A83-01 (0.5 mmol/L; Cat. No. 2939, R&D Systems), and L-WRN conditioned medium containing Wnt3A, R-spondin 1, and mNoggin (SCM105, Sigma-Aldrich).

The organoid culture medium was completely refreshed every 3–4 days. Organoids were passaged weekly at a 1:3 to 1:6 split ratio by recovering them from Matrigel using BD Cell Recovery Solution (Cat. No. 354253, BD Biosciences) according to the manufacturer's instructions and transferring them to fresh Matrigel. Organoid numbers and sizes were quantified using ImageJ software (National Institutes of Health, NIH) [41].

2.9. Immunocytochemistry

$CD44^+$ or $CD133^+$ spheroids were fixed with 4% paraformaldehyde for 15 min, permeabilized with 0.1% Triton X-100 in phosphate-buffered saline (PBS) for 10 min, and blocked with 1% bovine serum albumin (BSA) in PBS for 1 h. The samples were incubated overnight at 4 °C with primary antibodies against fluorescein isothiocyanate (FITC)-conjugated CD44 (Cat. No. 130-113-334, Miltenyi Biotec), CD133 (FITC-conjugated; Cat. No. 130-110-968, Miltenyi Biotec), or SOX2 (Cat. No. 23064, Cell Signaling Technology). After washing, the samples were incubated with Alexa Fluor 488-, 594-, or 647–conjugated secondary antibodies (Cat. Nos. A-11008, A32744, and 32728 TR; Life Technologies). Nuclei were counterstained with 4′,6-diamidino-2-phenylindole (DAPI, Cat. No. F6057, Sigma-Aldrich). Images were acquired using a Zeiss confocal microscope and processed with Imaris software version 7.6.

2.10. Western blotting analysis

Total protein was extracted using RIPA buffer (Cat. No. Sc-24948, Santa Cruz Biotechnology, Dallas, TX, USA) containing protease and phosphatase inhibitors (Cat. No. 5872, Cell Signaling Technology, Danvers, MA, USA). Protein lysates (20 μg) were separated via sodium dodecyl-sulfate polyacrylamide gel electrophoresis and transferred onto nitrocellulose membranes. The membranes were blocked and incubated overnight at 4 °C with primary antibodies against CD44 (Cat. A1351, Abclonal; Cat. 3570, Cell Signaling), CD133 (sc-365,537, Santa Cruz), SOX2 (Cat. 23,064, Cell Signaling), OCT4 (Cat. A7920, Abclonal), NANOG (Cat. A22625, Abclonal), ALDHA1 (Cat. 54,135, Cell Signaling), KLF (Cat. 51,221, Cell Signaling), phosphor-p44/42 MAPK (Erk1/2) (Cat. 4370, Cell Signaling), ERK1 (sc-376,852, Santa Cruz), Phospho-SAPK/JNK (Thr183/Tyr185) (Cat. 4668, Cell Signaling), JNK1 (sc-1648, Santa Cruz), Phospho-p38 MAPK (Thr180/Tyr182) (Cat. 4511, Cell Signaling), p38 MAPK (Cat. 9212, Cell Signaling), cleaved Caspase-3 (Cat. 9661, Cell Signaling), and β-actin (Cat. MAB8929, R&D system). After incubation with horseradish peroxidase-conjugated secondary antibodies, immunoreactive bands were visualized using an enhanced chemiluminescence substrate (Cat. No. LF-QC01060, AbFrontier, Baileys Harbor, WI, USA).

2.11. Mouse xenograft models

All animal experiments were conducted in accordance with protocols approved by the Institutional Animal Care and Use Committee (IACUC) of Kangbuk Samsung Hospital (Approval No. 25-144-A1-N). For

subcutaneous xenograft assays, 5×10^6 $CD44^+$ or $CD133^+$ organoid-derived cells suspended in 100 μL of PBS:Matrigel mixture (v/v, 1:5) were injected subcutaneously into the flanks of six-week-old NOD/SCID mice. Tumor growth was monitored every three days using digital calipers, and tumor volume was calculated using the following formula: (length × $width^2$)/2.

2.12. Immunofluorescence (IF)

Formalin-fixed paraffin-embedded xenograft and lung metastasis tissues were sectioned at 3-μm thickness. Thereafter, sections were deparaffinized, rehydrated, and subjected to heat-induced antigen retrieval in citrate buffer (pH 6.0; Cat. No. 005000, Invitrogen). After blocking with 1% BSA, sections were incubated overnight at 4 °C with primary antibodies against CD44 (Cat. No. 3570, Cell Signaling Technology), CD133 (Cat. No. 64326, Cell Signaling Technology), SOX2 (Cat. No. 14962, Cell Signaling Technology), phosphor-p44/42 MAPK (Erk1/2) (Cat. 4370, Cell Signaling), or cleaved caspase-3 (Cat. No. 9661, Cell Signaling Technology).

After washing, sections were incubated with Alexa Fluor 488-, 594-, or 647–conjugated secondary antibodies (Cat. Nos. A-11008, A32744, and A32728TR; Life Technologies). Nuclei were counterstained with DAPI (Cat. No. F6057, Sigma-Aldrich), and slides were mounted for imaging. Images were captured using a Zeiss confocal microscope under identical acquisition settings. Quantitative analysis was performed on at least 5 randomly selected high-power fields per sample using Imaris software version 7.6 or ImageJ.

2.13. Statistical analysis

Data are presented as mean ± standard deviation (SD), unless otherwise indicated. All experiments were performed with at least three independent biological replicates ($n \geq 3$). For experiments involving technical repeats, values were averaged prior to statistical analysis.

Statistical significance was determined using unpaired two-tailed Student's t-test for comparisons between two groups, or one-way analysis of variance (ANOVA) followed by Tukey's post hoc test for multiple comparisons. For non-parametric data, the Wilcoxon rank-sum test was applied as appropriate.

Effect sizes (mean differences between groups) and corresponding 95% confidence intervals (CIs) were calculated where applicable. Statistical significance was defined as $P < 0.05$.

GraphPad Prism 9 (GraphPad Software), ImageJ (NIH), Microsoft Excel, and R (ggplot 2 package) were used for data analysis and visualization.

3. Results

3.1. Structure-based interaction of UR-1 with CD44 and CD133 cancer stem-like cell markers

Structure-based molecular docking analyses were conducted to investigate the potential interaction of UR-1 with the cancer stem cell-associated surface markers CD44 and CD133. As shown in Fig. 1A, the overall workflow illustrates the structural design and chemical construction process of the UR-1 compound. As shown in Fig. 1A, the overall workflow illustrates the structural design and chemical construction process of the UR-1 compound. Three-dimensional structural models of CD44 and CD133 revealed well-defined ligand-accessible pockets suitable for small-molecule binding. Furthermore, docking simulations demonstrated that UR-1 favorably occupies a surface-exposed binding cavity within CD44, thereby forming stable interactions with surrounding residues through hydrogen bonding and hydrophobic contacts. The ligand was positioned deeply within the CD44 pocket, which suggests a strong binding affinity capable of modulating CD44-associated stemness functions (Fig. 1B, upper panel). Similarly, UR-1 exhibited a stable binding conformation within a predicted ligand-binding pocket of CD133. The docking pose revealed tight accommodation of UR-1 within the CD133 surface groove, which was supported by complementary shape fitting and non-covalent interactions (Fig. 1B, lower panel). Comparative docking score analysis further indicated that UR-1 displays comparable or slightly enhanced binding affinity toward CD133 relative to CD44, thus supporting its potential to broadly target multiple cancer stem cell-associated markers (Fig. 1C).

To functionally validate these predictions, spheroid culture conditions were established to enrich cancer stem-like cell populations, as confirmed in Supplementary Fig. S1A. Under these CSC-enriched conditions, CD44, CD133 and SOX2 expression were consistently upregulated across all cell lines, whereas other stemness-associated markers showed variable expression limited to one or two cell lines. These results indicate that cancer stem-like cells were successfully enriched under the spheroid culture conditions (Suppl. Fig. S1B).

UR-1 treatment exerted only modest effects in monolayer cultures and non–cancer stem-like cells (Suppl. Fig. S1C and S1D; Fig. 1D). In contrast, under CSC-enriched spheroid conditions, UR-1 exhibited markedly enhanced anti-tumor efficacy (Fig. 1E). This increased sensitivity was predominantly observed in $CD44^+$ and $CD133^+$ populations, whereas CD44-low/CD133-low non–stem-like cells showed limited responsiveness. These findings indicate that UR-1 displays preferential activity against cancer stem-like cells. Quantitative analyses further confirmed that $CD44^+$ and $CD133^+$ cells exhibited significantly greater reductions in viability and stemness-associated phenotypes upon UR-1 treatment (Fig. 1D and E).

Collectively, these findings, together with structure-based docking predictions, suggest a potential interaction between UR-1 and CD44/CD133 via surface-accessible binding sites. However, it should be noted that these predictions are derived from in silico modeling and do not constitute direct experimental evidence of binding. In addition, the present study does not directly establish the binding specificity of UR-1 toward CD44 or CD133 relative to unrelated membrane proteins. Therefore, the specificity of UR-1 interactions with CSC-associated markers is inferred from docking predictions and functional phenotypes but remains to be experimentally validated. Accordingly, whether UR-1 directly engages CD44/CD133 or modulates cancer stemness through downstream signaling pathways remains to be determined. Nonetheless, these results provide a conceptual framework for future studies aimed at experimentally validating target engagement and elucidating the underlying mechanisms of UR-1–mediated *anti*-stemness effects.

3.2. UR-1 suppresses stemness and self-renewal in $CD44^+$ cancer spheroids across multiple cancer types

$CD44^+$ cells were isolated from spheroid cultures to establish cancer stem–like populations for downstream analyses. The workflow involves enrichment of $CD44^+$ cells followed by their culture under three-dimensional conditions to generate spheroids and organoid-like structures, providing an experimental platform to evaluate the effects of UR-1. (Fig. 2A). Immunoblot analysis was performed to verify the successful enrichment of $CD44^+$ cells following isolation, showing increased CD44 expression in the sorted populations compared with controls (Fig. 2B). Cell proliferation assay was performed to assess the effects of UR-1 in $CD44^+$ cells. UR-1 treatment resulted in a dose-dependent decrease in proliferation, with a more pronounced inhibitory effect observed in $CD44^+$ populations across all three cancer models (Fig. 2C).

UR-1 substantially impaired spheroid-forming capacity in $CD44^+$ cells derived from SCC-15, N87, and MDA-MB-231. Representative bright-field images showed a reduction in spheroid size and loss of compact structure following UR-1 treatment across all cancer models. Quantitative analysis further confirmed a significant decrease in spheroid formation efficiency in UR-1-treated $CD44^+$ cells compared with controls (Fig. 2D), whereas $CD44^-$ populations exhibited no

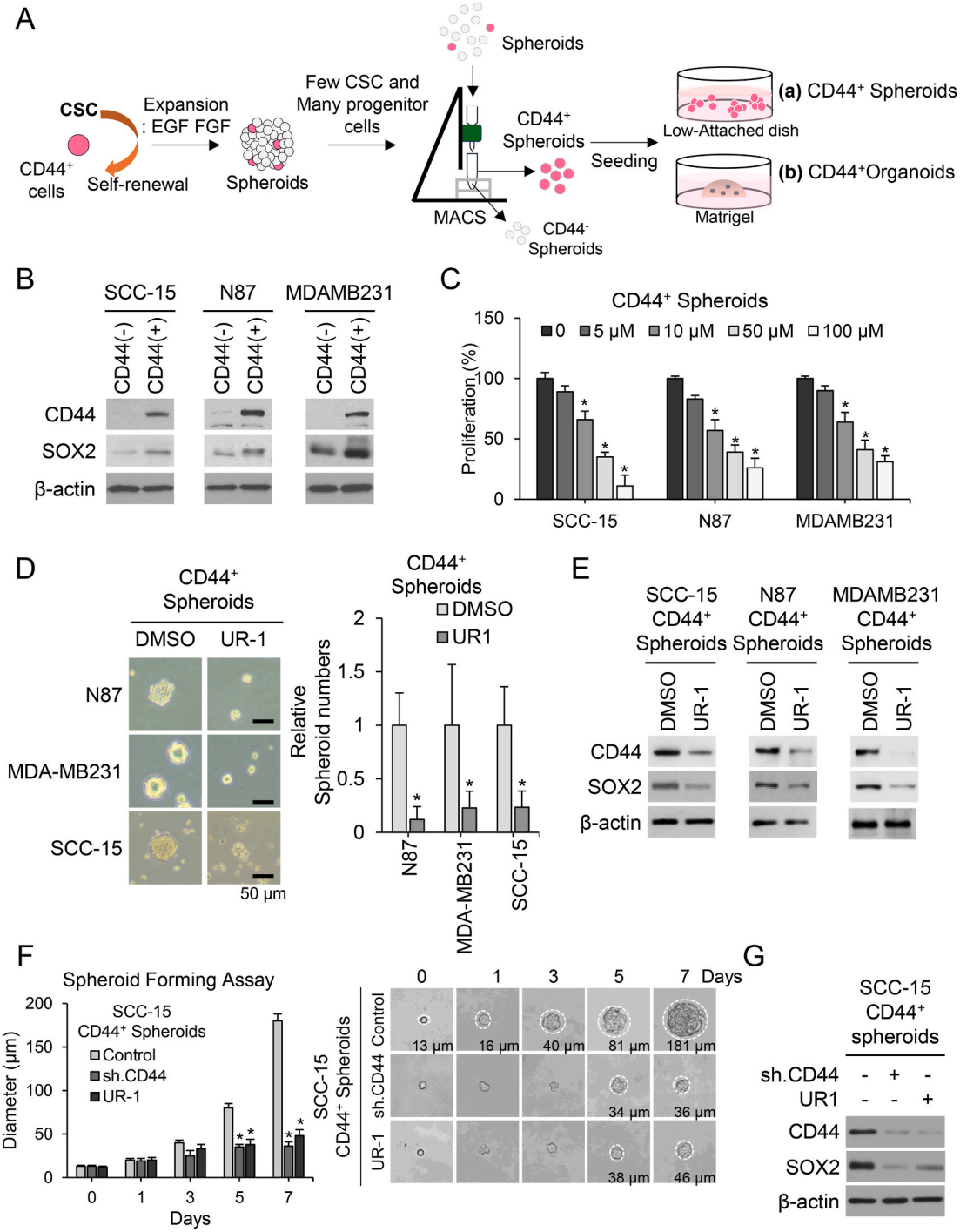


Fig. 2. UR-1 selectively suppresses stemness-associated protein expression and three-dimensional growth of CD44$^+$ cancer stem-like cells. (A) Schematic illustration of the experimental workflow showing enrichment of CD44$^+$ cancer stem-like cells from SCC-15, N87, and MDA-MB-231 cell lines, followed by UR-1 treatment and evaluation using three-dimensional spheroid/organoid culture systems and molecular analyses. (B) Immunoblot analysis confirming enrichment of CD44$^+$ cells and demonstrating the expression of stemness-associated proteins in the indicated cancer cell lines. (C) Cell proliferation assays showing a dose-dependent decrease in proliferation following UR-1 treatment, with a more pronounced inhibitory effect observed in CD44$^+$ cancer cells across all three models. (D) Representative bright-field images and quantitative analysis of spheroid formation in CD44$^+$ cells under spheroid-forming conditions. UR-1 treatment markedly reduced spheroid size and formation efficiency compared with untreated controls, suggesting impaired self-renewal capacity in CSC-enriched populations. (E) Immunoblot analysis of CD44$^+$ cells showing that UR-1 treatment markedly reduces the expression of stemness-associated proteins compared with untreated controls. (F) Single-cell–derived spheroid formation assay in CD44$^+$ cells. Representative images and quantitative analysis show impaired self-renewal capacity and reduced spheroid growth following UR-1 treatment. (G) Immunoblot analysis of CD44$^+$ cells following UR-1 treatment demonstrating reduced expression of stemness-associated proteins compared with control and CD44 knockdown (sh.CD44) cells. Representative blots are shown. All quantitative data are presented as mean ± standard deviation (SD) from three independent biological replicates (n = 3). Statistical significance was determined using Student's t-test for comparisons between two groups or one-way ANOVA followed by Tukey's post hoc test for multiple comparisons. Representative blots are shown. P values are indicated as $P < 0.05$. Scale bars indicate the indicated magnification.

significant changes in spheroid formation or morphology upon UR-1 treatment (Suppl. Fig. S2A). Immunoblot analysis demonstrated that UR-1 treatment markedly reduced the expression of stemness-associated proteins in CD44$^+$ spheroids across all three cancer cell lines compared with that of untreated controls (Fig. 2E), thereby suggesting associated with impaired stemness-related phenotypes.

To further examine the relationship between CD44 expression and UR-1 responsiveness, CD44 overexpression was performed in SCC-15 cells. Immunoblot analysis confirmed successful overexpression of CD44 (Suppl. Fig. S2B). Under these conditions, CD44-overexpressing cells exhibited a greater reduction in viability upon UR-1 treatment compared with control cells, as shown by quantitative analysis (Suppl. Fig. S2C).

To assess self-renewal capacity under spheroid conditions, a single

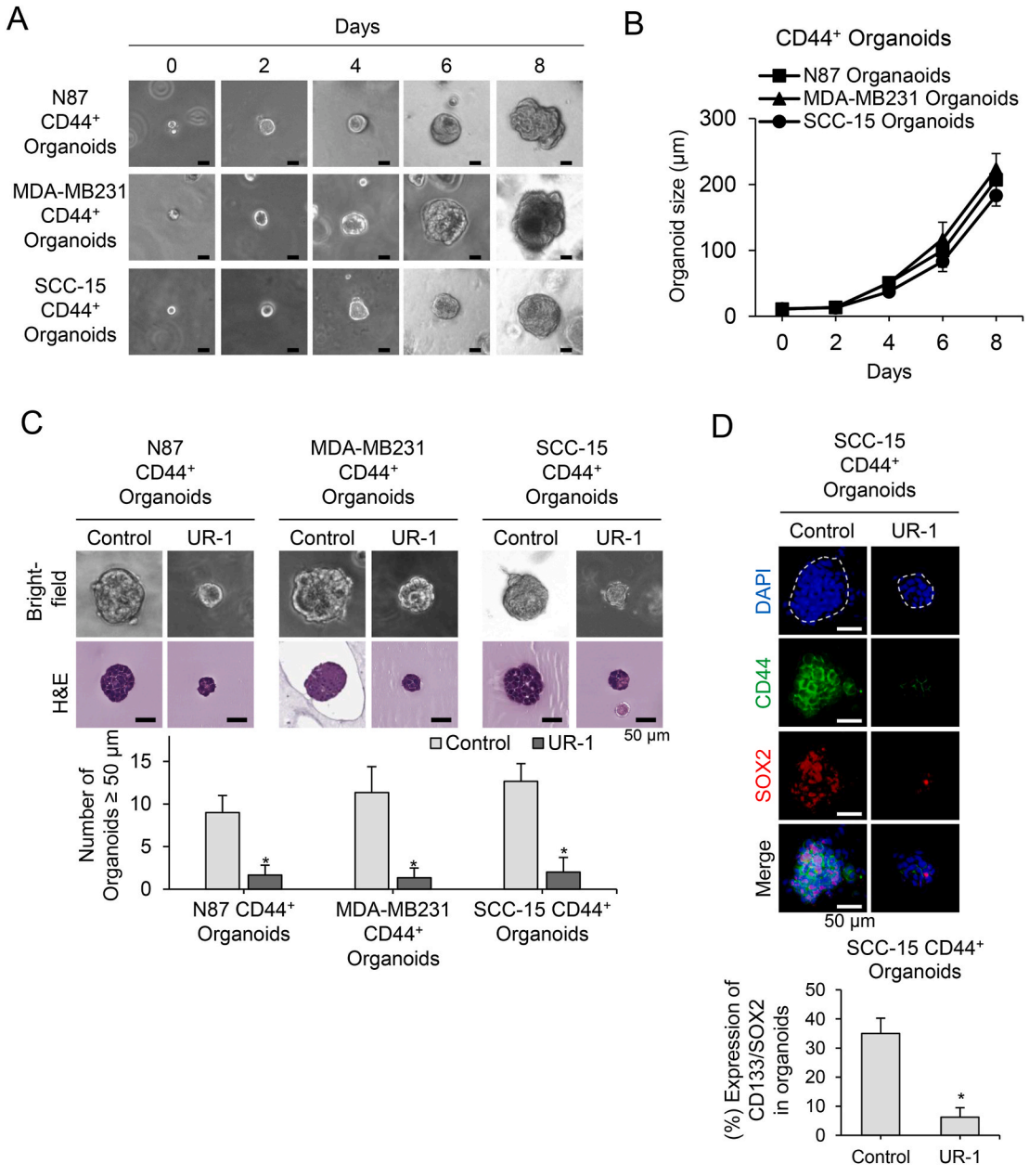


Fig. 3. UR-1 suppresses organoid growth and stemness marker expression in organoids derived from CD44$^+$ cancer stem-like cells. (A) Representative bright-field images showing the establishment and growth of three-dimensional organoids derived from CD44$^+$ spheroid-derived cells at the indicated time points under control conditions. Organoids exhibit progressive growth and well-defined structures over time. (B) Quantitative analysis of organoid growth corresponding to (A), demonstrating time-dependent expansion of organoids derived from CD44$^+$ cells under control conditions. (C) Upper panels: Representative bright-field images showing reduced organoid size and structural complexity following UR-1 treatment compared with untreated controls. Lower panels: Hematoxylin and eosin (H&E) staining of organoid sections. UR-1-treated organoids display reduced cellular density, disrupted epithelial organization, and compromised structural integrity relative to well-organized control organoids. Quantitative analysis confirms a significant reduction in organoid growth upon UR-1 treatment. (D) Immunofluorescence staining of organoids for stemness-associated markers CD44 (green) and SOX2 (red), with nuclei counterstained with DAPI (blue). Representative images show reduced CD44 and SOX2 expression in UR-1-treated organoids compared with controls. Quantitative analysis further confirms a significant decrease in marker expression following UR-1 treatment. All quantitative data are presented as mean ± standard deviation (SD) from three independent biological replicates (n = 3). Statistical significance was determined using Student's t-test for comparisons between two groups or one-way ANOVA followed by Tukey's post hoc test for multiple comparisons. P values are indicated as $P < 0.05$. Scale bars indicate the indicated magnification. (For interpretation of the references to color in this figure legend, the reader is referred to the Web version of this article.)

CD44$^+$ cell spheroid formation assay was performed. Compared with sh. CD44 cells, UR-1–treated cells showed a further reduction in spheroid growth, suggesting impaired expansion capacity (Fig. 2F). Quantitative analysis demonstrated that both UR-1 treatment and CD44 knockdown reduced spheroid growth and formation efficiency; notably, UR-1–treated cells exhibited a more pronounced inhibitory effect compared with sh. CD44 cells (Fig. 2F). Representative bright-field images supported these findings, showing smaller and less compact spheroids in UR-1–treated cells relative to sh. CD44 cells (Fig. 2F). Consistent with the single-cell spheroid assay results, immunoblot analysis demonstrated that UR-1 treatment markedly reduced the expression of the stemness-associated marker SOX2 While CD44 knockdown alone also decreased SOX2 levels, UR-1 treatment exerted a more pronounced inhibitory effect, supporting its superior efficacy in suppressing cancer stem-like properties (Fig. 2G).

Overall, UR-1 reduced spheroid formation and stemness-associated protein expression in CD44$^+$ cancer spheroid models derived from SCC-15, N87, and MDA-MB-231 cells, and enhanced responsiveness was observed in CD44-overexpressing conditions.

3.3. UR-1 inhibits organoid formation and stemness marker expression in CD44$^+$ cell-derived organoid models

Building on the suppressive effects of UR-1 observed in CD44$^+$ cancer spheroid models (Fig. 2), the effects of UR-1 were further evaluated in more physiologically relevant three-dimensional organoid systems. CD44$^+$ Organoids were established from SCC-15, N87, and MDA-MB-231 cancer cell lines (Fig. 3A). Under control conditions, all three cell lines efficiently formed organoids, confirming their intrinsic organoid-forming capacity at the time points (Fig. 3B).

Bright-field imaging revealed that UR-1 treatment markedly impaired organoid growth across all three cancer models (Fig. 3C, upper). Compared with untreated controls, UR-1-treated cultures exhibited a pronounced reduction in organoid size, number, and structural complexity, suggesting a strong inhibitory effect on organoid-forming efficiency (Fig. 3C). UR-1-treated organoids exhibited not only reduced growth but also morphological alterations, characterized by loss of compact architecture and irregular structural features (Fig. 3C). Organoids derived from sh. CD44 cells also showed reduced growth, exhibiting a comparable level of suppressive effect to that of UR-1-treated organoids (Suppl. Fig. S3A). Histological analysis using hematoxylin and eosin (H&E) staining further revealed that UR-1-treated organoids displayed a similar degree of structural disruption compared with the sh. CD44 group (Fig. 3C, lower; Suppl. Fig. S3A). Consistent with these morphological and histological findings, immunofluorescence analysis demonstrated a marked decrease in the expression of stemness-associated markers in UR-1-treated organoids. Both CD44 and SOX2 signals were substantially reduced in intensity and in the proportion of marker-positive cells compared with controls (Fig. 3D). Quantitative assessment confirmed a significant reduction in CD44$^+$ and SOX2$^+$ cell populations following UR-1 treatment, suggesting effective attenuation of stemness-associated phenotypes within the organoid structures.

Collectively, these results demonstrate that UR-1 suppresses organoid growth, disrupts structural integrity, and downregulates key stemness markers in organoids derived from multiple cancer cell lines. These findings extend the *anti*-stemness effects of UR-1 from CD44$^+$ spheroid models to organoid systems and support its broad inhibitory activity against stemness-driven tumor growth across diverse cancer types.

3.4. UR-1 suppresses stemness and self-renewal in CD133$^+$ CSCs

To further validate the *anti*-stemness effects of UR-1 in an independent CD133$^+$ CSC population, a workflow was established for the isolation and evaluation of CD133$^+$ cells from A549, SW480, and HepG2 cell lines (Fig. 4A). CD133$^+$ cells were enriched and subsequently subjected to three-dimensional culture conditions for downstream functional and molecular analyses. To validate the enrichment of cancer stem–like populations under spheroid conditions, the expression of stemness-associated markers and related proteins was examined (Suppl. Fig. S1B). Immunoblot analysis confirmed increased expression of CSC-associated markers in spheroid cultures compared with monolayer cells, supporting the successful establishment of stem-like tumor cell populations (Suppl. Fig. S1B).

Immunoblot analysis confirmed successful enrichment of CD133$^+$ cells, showing increased CD133 expression compared with unsorted controls (Fig. 4B). UR-1 treatment resulted in a dose-dependent decrease in proliferation, with a more pronounced inhibitory effect observed in CD133$^+$ populations across all three cancer models (Fig. 4C). In contrast, CD133$^-$ cells showed no significant changes in proliferation following UR-1 treatment, suggesting minimal responsiveness (Suppl. Figs. S1D and S4A).

To further examine the relationship between CD133 expression and UR-1 responsiveness, CD133 overexpression was performed in HepG2 cells. Immunoblot analysis confirmed overexpression of CD133 (Fig. 4D). Under these conditions, CD133-overexpressing cells exhibited a greater reduction in viability upon UR-1 treatment compared with control cells (Fig. 4E).

To assess self-renewal capacity under spheroid conditions, a single CD133$^+$ cell spheroid formation assay was performed. Compared with sh. CD133 cells, UR-1–treated cells showed a further reduction in spheroid growth, suggesting impaired expansion capacity (Suppl. Fig. S4B). Quantitative analysis demonstrated that both UR-1 treatment and CD133 knockdown reduced spheroid growth and formation efficiency; notably, UR-1–treated cells exhibited a more pronounced inhibitory effect compared with sh. CD133 cells. Representative bright-field images supported these findings, showing smaller and less compact spheroids in UR-1–treated cells relative to sh. CD133 cells (Suppl. Fig. S4B). Inhibition efficiency was confirmed (Suppl. Fig. S4C).

Consistent with these molecular changes, UR-1 substantially impaired the spheroid-forming capacity of CD133$^+$ cells derived from A549, SW480, and HepG2. Representative bright-field images showed no appreciable changes in spheroid size or morphology in CD133$^-$ cells following UR-1 treatment, whereas CD133$^+$ cells exhibited a clear reduction in spheroid size and loss of compact structure (Fig. 4F). Quantitative analysis further confirmed a significant decrease in spheroid formation efficiency in UR-1-treated CD133$^+$ cells compared with controls (Fig. 4F). Consistent with these phenotypic effects, immunoblot analysis of CD133$^+$ spheroids revealed a marked reduction in the expression of stemness-associated proteins following UR-1 treatment (Fig. 4G).

These results demonstrate that UR-1 suppresses stemness-associated molecular expression and three-dimensional growth capacity in CD133$^+$ CSCs derived from lung, colorectal, and liver cancers. By consistently inhibiting stemness-related features across multiple cancer types and three-dimensional culture systems, UR-1 extends its *anti*-stemness activity beyond CD133$^+$ populations and highlights a broader impact on the maintenance of CSC phenotypes.

3.5. UR-1 suppresses organoid growth and stemness marker expression in CD133$^+$ cancer organoid models

CD133$^+$ cancer organoids were established and analyzed to determine the impact of UR-1 on organoid growth and stemness-associated features (Fig. 5A). Under organoid-forming conditions, CD133$^+$ cells consistently generated well-organized, compact, and multilayered organoid structures, whereas CD133$^-$ cells produced smaller and poorly organized organoids (Fig. 5B). This highlights the enhanced organoid-forming capacity of CD133$^+$ populations.

Exposure to UR-1 resulted in pronounced suppression of CD133$^+$ organoid growth. Bright-field imaging revealed a clear reduction in

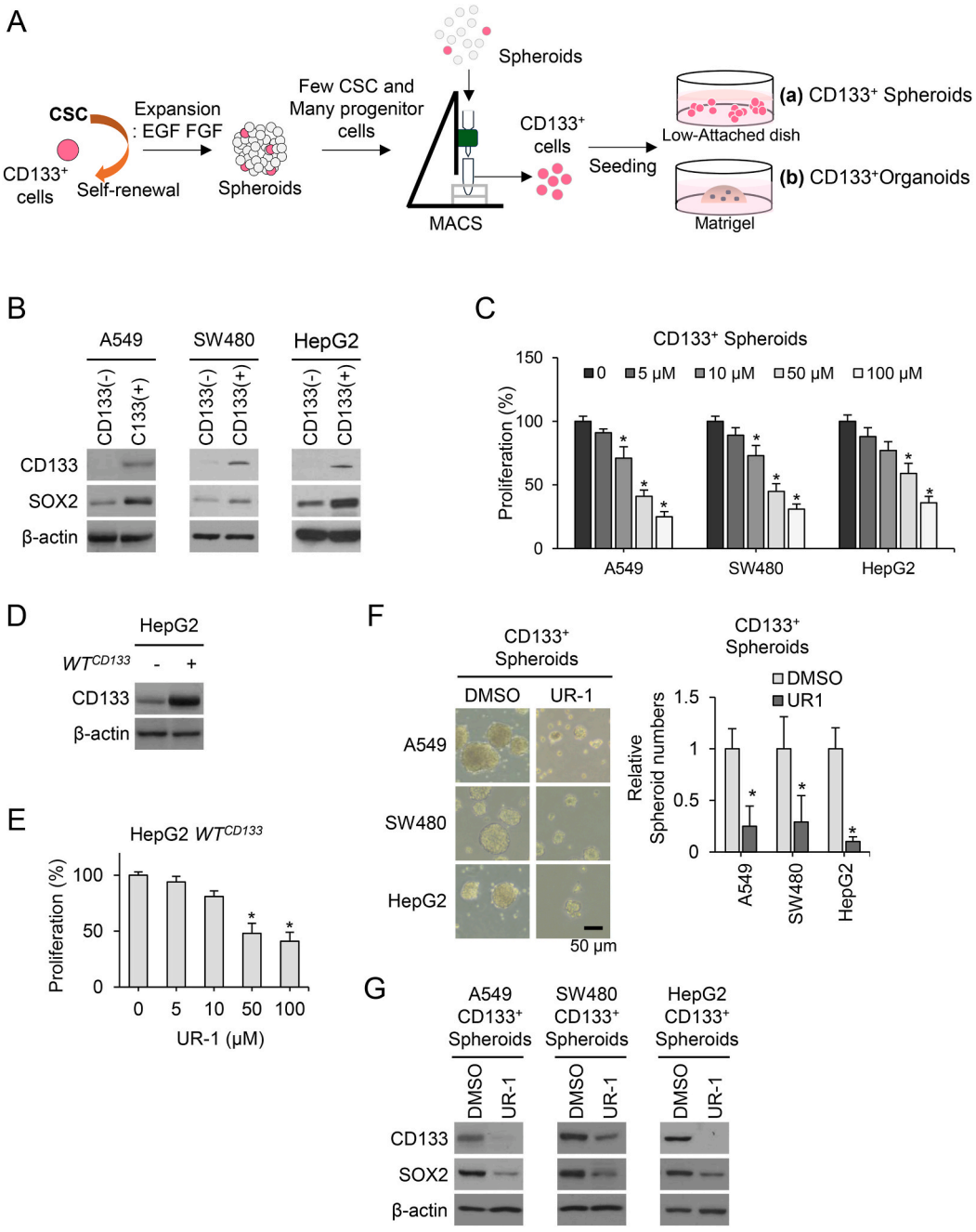


Fig. 4. UR-1 suppresses stemness-associated properties in CD133$^+$ cancer stem-like cell models. (A) Schematic illustration of the experimental workflow for enrichment of CD133$^+$ cancer stem-like cells from A549, SW480, and HepG2 cell lines, followed by UR-1 treatment and evaluation using three-dimensional spheroid-forming assays and molecular analyses. (B) Immunoblot analysis confirming enrichment of CD133$^+$ cells and increased expression of stemness-associated proteins under spheroid-forming conditions. Representative blots are shown. (C) Cell proliferation assays demonstrating a dose-dependent decrease in proliferation following UR-1 treatment, with a more pronounced inhibitory effect observed in CD133$^+$ cancer cells across all three models. (D) Immunoblot analysis of CD133 expression in HepG2 cells (monolayer) following CD133 overexpression. Representative blots are shown. (E) Cell proliferation assays in HepG2 cells (monolayer) showing that CD133-overexpressing cells exhibit increased sensitivity to UR-1 treatment, as evidenced by a greater reduction in cell viability compared with control cells. Quantitative analysis is shown.(C) Cell proliferation assays demonstrating a dose-dependent decrease in proliferation following UR-1 treatment, with a more pronounced inhibitory effect observed in CD133$^+$ cancer cells across all three models. (D) Immunoblot analysis of CD133 expression in HepG2 cells (monolayer) following CD133 overexpression. Representative blots are shown. (E) Cell proliferation assays in HepG2 cells (monolayer) showing that CD133-overexpressing cells exhibit increased sensitivity to UR-1 treatment, as evidenced by a greater reduction in cell viability compared with control cells. Quantitative analysis is shown. (F) Representative bright-field images and quantitative analysis of spheroid formation in CD133$^+$ cells, demonstrating that UR-1 treatment significantly reduces spheroid size and formation efficiency compared with untreated controls, suggesting impaired self-renewal capacity. (G) Immunoblot analysis of CD133$^+$ spheroids showing decreased expression of stemness-associated proteins following UR-1 treatment compared with control cells. All quantitative data are presented as mean ± standard deviation (SD) from three independent biological replicates (n = 3). Statistical significance was determined using Student's t-test for comparisons between two groups or one-way ANOVA followed by Tukey's post hoc test for multiple comparisons. Representative blots are shown. P values are indicated as $P < 0.05$. Scale bars indicate the indicated magnification.

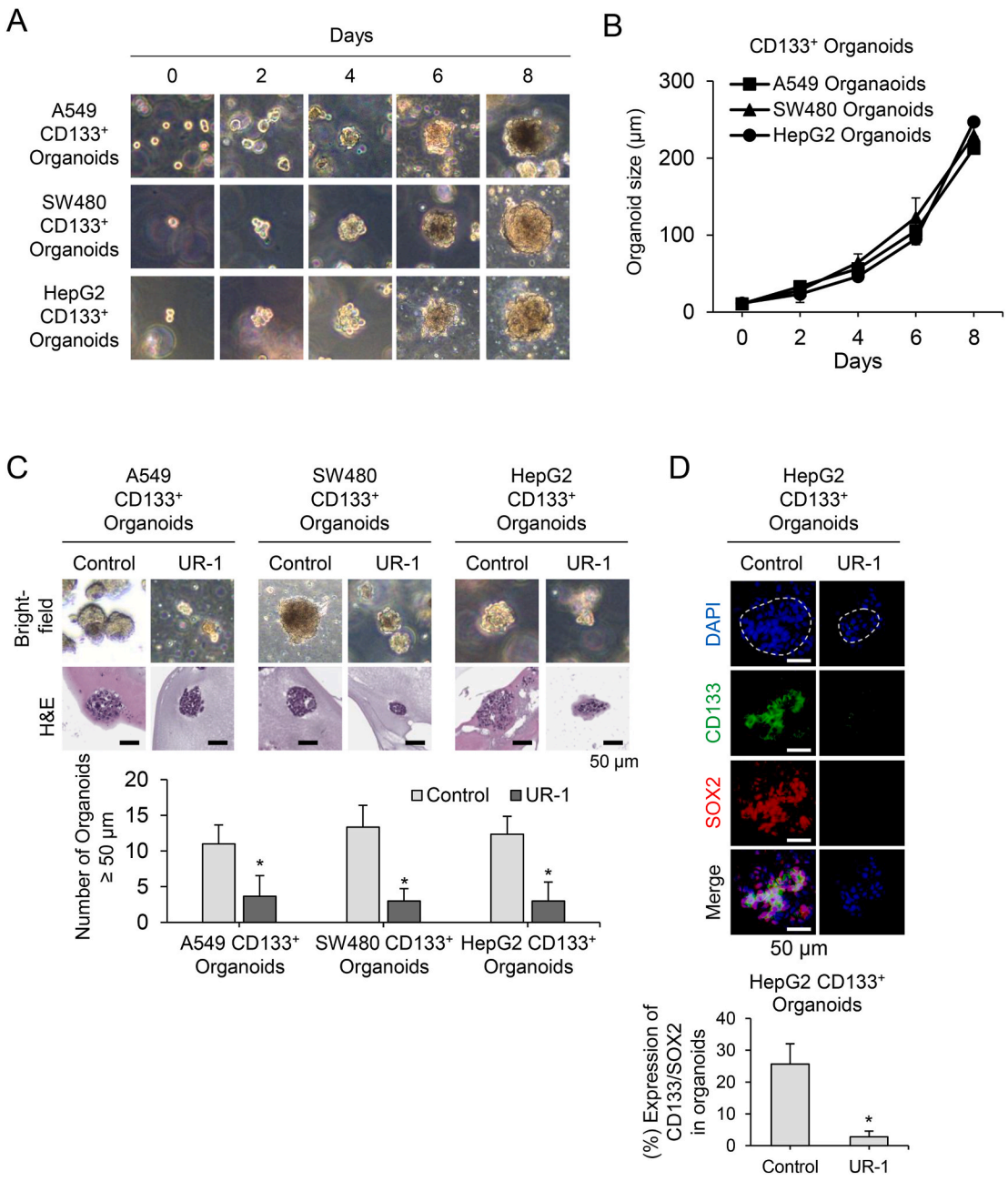


Fig. 5. UR-1 inhibits organoid growth and stemness marker expression in CD133$^+$ cancer organoid models. (A) Representative bright-field images showing the establishment and progression of three-dimensional organoids derived from CD133$^+$ cells isolated from spheroids at the indicated time points. The CD133$^+$-derived organoids exhibited robust growth and progressively increased structural complexity under control conditions. (B) Quantitative analysis of organoid growth over time corresponding to the cultures shown in (A), demonstrating progressive expansion of CD133$^+$-derived organoids. (C) Upper panels: Representative bright-field images showing reduced organoid size and impaired structural development following UR-1 treatment compared with untreated controls. Lower panels: Hematoxylin and eosin (H&E) staining of organoid sections showing decreased cellular density and disrupted internal architecture in UR-1-treated organoids. (D) Immunofluorescence staining of organoids for stemness-associated markers CD133 (green) and SOX2 (red), with nuclei counterstained with DAPI (blue). UR-1 treatment reduced CD133 and SOX2 expression compared with control organoids. Quantitative analysis of fluorescence intensity is shown, confirming a significant decrease in stemness marker expression upon UR-1 treatment. Data are presented as mean ± SD from three independent experiments (n = 3). Statistical significance was determined using Student's t-test or one-way ANOVA followed by Tukey's post hoc test, as appropriate (*P < 0.05). Scale bars are as indicated. (For interpretation of the references to color in this figure legend, the reader is referred to the Web version of this article.)

organoid size, number, and overall structural complexity in UR-1-treated CD133$^+$ organoids compared with that in untreated controls (Fig. 5C). Organoids derived from sh. CD133 cells also showed reduced growth. However, UR-1–treated CD133$^+$ organoids exhibited a comparable inhibitory effect to that observed in sh. CD133 cells (Suppl. Fig. S5A). In addition to reduced growth, UR-1-treated organoids displayed irregular borders and loss of compact architecture, which indicated compromised organoid integrity. Histological analysis further supported these observations. UR-1-treated CD133$^+$ organoids exhibited reduced cellular density and disrupted internal organization relative to controls and sh. CD133 groups, which suggested impaired cellular cohesion and diminished three-dimensional organization within the organoid structures (Fig. 5C). These architectural alterations were consistently observed across independent experiments. Consistent with

the observed morphological and histological changes, immunofluorescence analysis demonstrated a marked decrease in stemness-associated marker expression in CD133$^+$ organoids following UR-1 treatment (Fig. 5D). Both CD133 and SOX2 signals were substantially reduced in intensity and distribution compared with untreated organoids, suggesting a loss of stemness-associated cellular features within the three-dimensional context.

These findings demonstrate that UR-1 effectively suppresses organoid growth, architectural organization, and stemness marker expression in CD133$^+$ cancer organoid models. These results further support the inhibitory effect of UR-1 on stemness-driven tumor growth in three-dimensional systems and reinforces its activity across distinct CSC populations.

3.6. *UR1 inhibits ERK signaling in CD44$^+$ and CD133$^+$ populations*

The ERK/MAPK pathway has been widely reported to promote CSC self-renewal, survival, and tumor-initiating capacity across multiple cancer types [7–9]. In particular, activation of ERK signaling has been associated with the maintenance of stemness markers and resistance to therapy in CSC populations [7–9].

To investigate the mechanism by which UR-1 regulates CD44$^-$and CD133-associated stemness, we examined MAPK signaling pathways in CD44$^-$ and CD44$^+$ cell populations derived from spheroids of SCC-15 and HepG2 cells. In CD44$^+$ and CD133$^+$ cells, phosphorylation of ERK (pERK) was elevated, whereas phosphorylation of JNK (pJNK) showed a modest increase and phosphorylation of p38 (p-p38) remained unchanged (Suppl. Fig. S6A), suggesting preferential activation of the ERK pathway. Consistent with this, UR-1 treatment markedly reduced ERK phosphorylation without significantly affecting total ERK levels, suggesting suppression of ERK pathway activation (Suppl. Fig. S5A–S5B). In contrast, UR-1 had minimal effects on pJNK and p-p38 levels, supporting a selective inhibitory effect on ERK signaling. This inhibition of ERK signaling was accompanied by decreased expression of stemness-associated markers, including CD44, CD133, and SOX2 (*Data not* shown). Functionally, UR-1 treatment significantly impaired organoid formation capacity, as evidenced by smaller and less compact organoids compared with controls. Functionally, UR-1 treatment significantly impaired organoid formation capacity, as evidenced by smaller and less compact organoids compared with controls.

Collectively, these findings suggest that UR-1 suppresses cancer stem-like properties, at least in part, through selective inhibition of ERK signaling.

3.7. *UR-1 suppresses stemness marker expression and induces apoptotic signaling in CD44$^+$ and CD133$^+$ organoid-derived xenografts*

We next established xenograft tumors using CD44$^+$ or CD133$^+$ cancer organoids to evaluate the *in vivo* effects of UR-1 on stemness-associated features, as organoid-derived xenograft models closely recapitulate patient tumor architecture, cellular heterogeneity, and therapeutic response, thereby providing enhanced translational and clinical relevance compared with conventional cell line–based xenografts [42]. Tumors derived from CD44$^+$ and CD133$^+$ organoids exhibited robust growth and retained strong expression of stemness markers, which confirmed the preservation of stem-like characteristics from the parental organoids (Fig. 6A and B).

Immunofluorescence analysis of xenograft tissues revealed marked changes in stemness and apoptotic marker expression following UR-1 treatment. Control tumors displayed prominent CD44 or CD133 staining accompanied by strong SOX2, and p-ERK1/2 protein expression, thereby suggesting maintenance of stem-like properties within the tumor tissues (Fig. 6C and D). In contrast, UR-1-treated xenografts showed a substantial reduction in CD44$^+$ and CD133$^+$ cell populations together with a pronounced decrease in SOX2 and p-ERK protein expression, thus reflecting attenuation of stemness-associated phenotypes *in vivo*. Concomitantly, UR-1 treatment led to a clear increase in cleaved caspase-3-positive cells within xenograft tumors. Cleaved Caspase-3 signals were sparse in control tumors but markedly elevated in UR-1-treated xenografts, thereby suggesting activation of apoptotic signaling. Spatially, regions exhibiting reduced stemness marker expression frequently overlapped with areas showing enhanced cleaved Caspase-3 staining. This suggests coordinated suppression of stemness and induction of apoptosis. Quantitative analysis further confirmed a pronounced reduction in the proportion of CD44$^+$/SOX2$^+$ or CD133$^+$/SOX2$^+$ cells following UR-1 treatment, accompanied by a corresponding increase in cleaved Caspase-3-positive cells.

These findings demonstrate that UR-1 effectively suppresses stemness-associated marker expression while promoting apoptotic signaling in CD44$^+$ and CD133$^+$ organoid-derived xenografts. This effectively extends its *anti*-stemness activity from *in vitro* organoid models to *in vivo* tumor systems.

4. Discussion

CD44 and CD133 have been widely recognized as key markers of CSC populations and are increasingly regarded as critical therapeutic targets in diverse solid malignancies [9–11,17]. CD44 is a cell-surface glycoprotein involved in cell adhesion, migration, and tumor–microenvironment interactions. The Glycoprotein plays a central role in maintaining CSC self-renewal capacity and promoting invasion and metastasis. Consequently, CD44$^+$ tumor cells are consistently enriched following chemotherapy and radiotherapy and exhibit heightened resistance to cytotoxic stress, thereby implicating them as a major cellular source of tumor recurrence [20,23,43].

Correspondingly, CD133 is a pentaspan transmembrane protein associated with stem cell-like phenotypes. The protein has been strongly linked to tumor-initiating capacity, three-dimensional spheroid and organoid formation, and poor clinical prognosis across multiple cancer types [19,44,45]. CD133$^+$ CSCs display enhanced DNA damage repair, resistance to oxidative stress, and activation of anti-apoptotic signaling pathways, rendering them refractory to conventional anticancer therapies [7,18,46]. Notably, CSC populations co-expressing CD44 and CD133 exhibit even greater tumorigenicity and therapeutic resistance than that of single-marker-positive cells. This emphasizes their role as high-risk subpopulations that drive disease persistence and relapse [19,21,47–51].

Given these functional attributes, CD44$^+$ and CD133$^+$ CSCs represent compelling therapeutic targets for overcoming the limitations of current anticancer strategies. Therefore, approaches that selectively eliminate or functionally impair these CSC populations have the potential to achieve more durable tumor control by addressing the cellular reservoirs responsible for therapy resistance, metastasis, and tumor recurrence. Accordingly, targeting CD44$^-$and CD133-defined CSC populations has emerged as a promising strategy to complement conventional treatments and improve long-term clinical outcomes [12].

Suitably, chalcone derivatives represent a versatile class of small molecules whose chemical architecture enables broad biological activity in cancer-related contexts [24,27,29,34]. The electrophilic α,β-unsaturated carbonyl moiety characteristic of chalcones facilitates interactions with regulatory proteins involved in redox balance, cell survival, and adaptive stress responses, thereby distinguishing these compounds from conventional cytotoxic agents that primarily target rapidly proliferating tumor cells [30,31]. Rather than exerting uniform antiproliferative effects, many chalcone-based compounds modulate signaling pathways associated with cellular plasticity and phenotypic heterogeneity. These signaling pathways are increasingly recognized as central drivers of tumor progression, therapy resistance, and disease recurrence.

Furthermore, chalcone derivatives regulate molecular programs linked to stemness maintenance and cell fate determination [29,31,33,34]. This suggests that chalcone-based compounds may preferentially

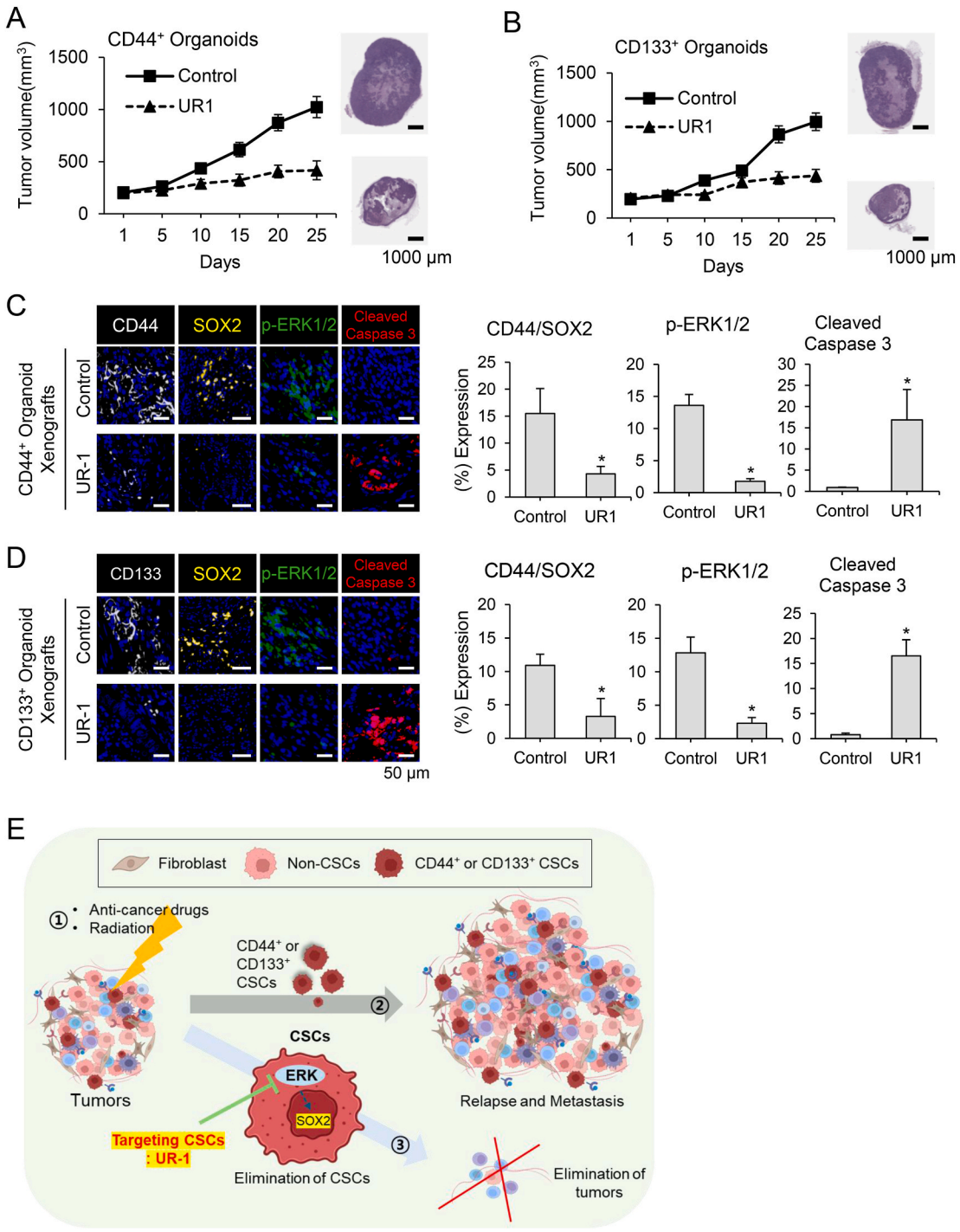


Fig. 6. UR-1 suppresses stemness marker expression and induces apoptotic signaling in CD44$^+$ and CD133$^+$ organoid-derived xenografts. (A–B) Tumor growth curves of xenografts established from CD44$^+$ and CD133$^+$ cancer organoids, showing that UR-1 treatment significantly suppresses tumor progression compared with vehicle-treated controls. (C) Representative immunofluorescence images of CD44$^+$ organoid-derived xenograft tumor sections stained for CD44 (green), SOX2 (white), phosphorylated ERK1/2 (p-ERK1/2, white), and cleaved caspase-3 (red), with nuclei counterstained with DAPI (blue). UR-1 treatment resulted in decreased CD44, SOX2, and p-ERK1/2 expression, accompanied by increased cleaved caspase-3 staining compared with control tumors. Quantitative analysis of marker expression is shown. Scale bars are as indicated. (D) Representative immunofluorescence images of CD133$^+$ organoid-derived xenograft tumor sections stained for CD133 (green), SOX2 (white), p-ERK1/2 (white), and cleaved caspase-3 (red), with DAPI counterstaining. UR-1-treated tumors exhibited reduced CD133, SOX2, and p-ERK1/2 expression and enhanced apoptotic signaling relative to controls. Quantitative analysis of fluorescence intensity for each marker is shown. Scale bars are as indicated. (E) Schematic model illustrating the proposed mechanism of UR-1 action. ① Conventional anticancer therapies (e.g., chemotherapy or radiation) preferentially eliminate non-stem tumor cells, while CD44$^+$ or CD133$^+$ cancer stem-like cells (CSCs) survive within the tumor. ② The residual CSC populations maintain stemness through activation of ERK signaling and downstream stemness-associated programs (e.g., SOX2), leading to tumor relapse and metastasis. ③ In contrast, UR-1 targets CSCs by suppressing ERK signaling and stemness-associated pathways while promoting apoptotic cell death, thereby eliminating CSCs and reducing tumor recurrence and progression. Data are presented as mean ± SD from at least three independent experiments (n = 3). Statistical significance was determined using Student's t-test or one-way ANOVA followed by Tukey's post hoc test, as appropriate (*P < 0.05). (For interpretation of the references to color in this figure legend, the reader is referred to the Web version of this article.)

affect CSC populations that contribute disproportionately to therapeutic resistance and tumor relapse. Such properties position chalcone derivatives as promising candidates for anticancer strategies aimed at suppressing tumor recurrence by targeting resilient cellular subpopulations that evade standard treatments.

Chalcones are a class of flavonoid-related compounds characterized by an α,β-unsaturated carbonyl scaffold, which functions as a reactive Michael acceptor. This structural feature enables chalcones to interact with nucleophilic residues, particularly cysteine thiols, in target proteins, thereby modulating key signaling pathways involved in cancer progression. Through these interactions, chalcones have been reported to regulate multiple oncogenic pathways, including MAPK/ERK, NF-κB, and PI3K/AKT signaling, leading to inhibition of cell proliferation, induction of apoptosis, and suppression of cancer stemness. Owing to these biochemical properties, chalcone derivatives have been widely investigated as promising anticancer agents in various cancer models [52–54].

Importantly, the present findings further identify inhibition of ERK phosphorylation (p-ERK) as a key mechanistic basis underlying the *anti*-stemness activity of UR-1. ERK signaling has been widely implicated in the regulation of CSC maintenance, self-renewal, and therapeutic resistance [10–12], and its persistent activation represents a critical driver of tumor aggressiveness. The ability of UR-1 to suppress p-ERK suggests that this compound is associated with modulation of a central signaling axis that sustains CSC phenotypes. By attenuating ERK-dependent stemness programs, UR-1 reduces the self-renewal capacity of $CD44^+$ and $CD133^+$ CSC populations and promotes apoptotic vulnerability, thereby overcoming a key limitation of conventional therapies. These findings highlight UR-1 as a functionally significant ERK-modulating agent with therapeutic potential in CSC-driven malignancies.

Although UR-1 consistently reduced ERK phosphorylation across multiple experimental models, the present study does not establish whether ERK is a direct molecular target of UR-1. Therefore, it remains possible that ERK inhibition occurs indirectly through upstream or parallel signaling pathways. Further biochemical and target-engagement studies will be required to determine the precise molecular mechanism underlying UR-1-mediated ERK suppression.

In this context, the structure-based analyses performed in the present study provide an additional mechanistic layer supporting the CSC-directed activity of UR-1. Molecular docking and binding affinity analyses revealed that UR-1 favorably interacts with surface-accessible binding pockets of both CD44 and CD133, with comparable affinity toward the two CSC markers. While these in silico and biochemical findings do not imply direct functional blockade of receptor signaling, they suggest that UR-1 is structurally compatible with CSC-associated surface proteins that define highly tumorigenic and therapy-resistant cell populations. This dual interaction profile may, at least in part, contribute to the broad *anti*-stemness effects of UR-1 observed across multiple tumor types and experimental systems.

Building on this conceptual framework, the current study demonstrates that UR-1, a novel chalcone-based compound, exerts robust antitumor activity by selectively targeting CSC populations defined by CD44 and CD133 expression. Across multiple aggressive solid tumor models, UR-1 consistently suppressed key CSC-associated phenotypes, including self-renewal capacity, three-dimensional spheroid and organoid formation, and tumor growth *in vivo*. These inhibitory effects were reproducibly observed in CSC-enriched spheroid cultures, patient-relevant organoid systems, and organoid-derived xenograft models, thereby supporting the broad and context-independent *anti*-stemness activity of UR-1. Importantly, the preferential reduction of $CD44^+$ and $CD133^+$ CSC populations, together with the preservation of non-stem-like cell viability at effective concentrations, suggests that UR-1 acts through a CSC-directed mechanism, rather than nonspecific cytotoxicity.

From a therapeutic perspective, this selective targeting of CSCs is of great importance as it addresses a central limitation of current anticancer therapies, which is the persistence of stem-like tumor cells that drive therapy resistance, tumor recurrence, and disease progression.

This study demonstrates that UR-1 robustly suppresses CSC properties across multiple complementary experimental platforms, including spheroid cultures, organoid models, and organoid-derived xenografts. UR-1 consistently impaired stemness maintenance in $CD44^+$ cancer spheroid and organoid models derived from diverse tumor origins, which indicates a broad *anti*-stemness activity that is not confined to a single cancer type. These effects were further validated in $CD133^+$ cancer organoids, where UR-1 markedly inhibited three-dimensional growth, disrupted structural organization, and downregulated stemness-associated marker expression.

Based on these findings, we propose a model in which conventional anti-cancer treatments preferentially eliminate non-stem tumor cells, while $CD44^+$ or $CD133^+$ cancer stem-like cells persist and contribute to tumor relapse and metastasis. These CSC populations are associated with activation of ERK signaling and maintenance of stemness-related programs. In this context, UR-1 is associated with reduced ERK activation and suppression of stemness-associated factors, thereby impairing CSC survival and self-renewal. Consequently, targeting CSCs with UR-1 may reduce tumor recurrence and improve overall therapeutic efficacy (Fig. 6E).

Importantly, the *anti*-stemness effect of UR-1 was recapitulated *in vivo* using organoid-derived xenograft models, in which UR-1 treatment markedly attenuated the stem-like characteristics of $CD44^+$ and $CD133^+$ tumor cells. The coordinated suppression of CD44, CD133, and SOX2 expression, together with increased cleaved Caspase-3 signaling, supports a dual mechanism involving stemness inhibition and apoptosis induction within CSC populations. These findings identify UR-1 as a promising chalcone-based analog with stemness-modulating activity and provide a rationale for further translational studies aimed at targeting CSCs to improve durable cancer control.

Patient consent for publication

Not applicable. This study did not involve human participants or patient-derived samples, and no identifiable patient data were included in the manuscript.

Ethics approval and consent to participate

This study did not involve human participants or patient-derived materials; therefore, Institutional Review Board (IRB) approval and informed consent were not required. All animal experiments were conducted in accordance with protocols approved by the Institutional Animal Care and Use Committee (IACUC), and human cell lines were handled following institutional biosafety and ethical guidelines.

Funding

This work was supported by the National Research Foundation of Korea (NRF), funded by the Ministry of Science and ICT (grant numbers RS-2023-00252049, RS-2024-00457100 , RS-2024-00339811 and RS-2026-25486519); the Korea–US Collaborative Research Fund (KUCRF) funded by the Ministry of Science and ICT and the Ministry of Health & Welfare, Republic of Korea (grant number RS-2024-00468,417); and the KBSMC–SKKU Future Clinical Convergence Academic Research Program (Kangbuk Samsung Hospital & Sungkyunkwan University).

CRediT authorship contribution statement

Suji Baek: Data curation, Formal analysis, Methodology, Resources, Software, Validation. **Seojin Jang:** Data curation, Formal analysis, Methodology, Resources, Validation, Visualization. **Sei Young Lee:** Data curation, Formal analysis, Methodology, Project administration,

Validation, Visualization. **Seo Lyn Choi:** Formal analysis, Methodology. **Jeong-Yoon Yang:** Methodology, Resources. **Jung Ho Park:** Formal analysis, Methodology. **Bom Sahn Kim:** Formal analysis, Methodology. **Seok-Hyung Kim:** Resources, Validation. **Jae Jun Lee:** Conceptualization, Formal analysis, Methodology, Resources. **Sang-Hyuk Lee:** Formal analysis, Methodology, Writing – review & editing. **Byung Seok Moon:** Conceptualization, Investigation, Project administration, Software, Writing – original draft. **Chang-Whan Yoon:** Conceptualization, Formal analysis, Project administration, Resources, Supervision, Validation, Writing – original draft. **Kang Pa Lee:** Conceptualization, Data curation, Investigation, Methodology, Resources, Supervision, Writing – original draft, Writing – review & editing.

Declaration of Competing Interest

The authors declare the following financial interests/personal relationships which may be considered as potential competing interests: Chang-Whan Yoon reports was provided by Kangbuk Samsung Hospital. If there are other authors, they declare that they have no known competing financial interests or personal relationships that could have appeared to influence the work reported in this paper.

Acknowledgments

We would like to thank Editage (www.editage.co.kr) for English language editing.

Appendix A. Supplementary data

Supplementary data to this article can be found online at https://doi.org/10.1016/j.yexcr.2026.115070.

Data availability

Data will be made available on request.

References

[1] R.L. Siegel, K.D. Miller, N.S. Wagle, A. Jemal, Cancer statistics, 2023, CA Cancer J. Clin. 73 (2023) 17–48.
[2] D. Hanahan, Hallmarks of cancer: new dimensions, Cancer Discov. 12 (2022) 31–46.
[3] I. Dagogo-Jack, A.T. Shaw, Tumour heterogeneity and resistance to cancer therapies, Nat. Rev. Clin. Oncol. 15 (2018) 81–94.
[4] P. Sharma, S. Hu-Lieskovan, J.A. Wargo, A. Ribas, Primary, adaptive, and acquired resistance to cancer immunotherapy, Cell 168 (2017) 707–723.
[5] S. Valastyan, R.A. Weinberg, Tumor metastasis: molecular insights and evolving paradigms, Cell 147 (2011) 275–292.
[6] Y. Li, Z. Wang, J.A. Ajani, S. Song, Drug resistance and cancer stem cells, Cell Commun. Signal. 19 (19) (2021).
[7] T. Shibue, R.A. Weinberg, EMT, CSCs, and drug resistance: the mechanistic link and clinical implications, Nat. Rev. Clin. Oncol. 14 (2017) 611–629.
[8] A. Mitra, L. Mishra, S. Li, EMT, CTCs and CSCs in tumor relapse and drug-resistance, Oncotarget 6 (2015) 10697–10711.
[9] E. Batlle, H. Clevers, Cancer stem cells revisited, Nat. Med. (N. Y., NY, U. S.) 23 (2017) 1124–1134.
[10] X. Chu, W. Tian, J. Ning, et al., Cancer stem cells: advances in knowledge and implications for cancer therapy, Signal Transduct. Targeted Ther. 9 (2024) 170.
[11] L.T.H. Phi, I.N. Sari, Y.G. Yang, et al., Cancer stem cells (CSCs) in drug resistance and their therapeutic implications in cancer treatment, Stem Cell. Int. 2018 (2018) 5416923.
[12] M.L. O'Connor, D. Xiang, S. Shigdar, et al., Cancer stem cells: a contentious hypothesis now moving forward, Cancer Lett. 344 (2014) 180–187.
[13] B.C. Prager, Q. Xie, S. Bao, J.N. Rich, Cancer stem cells: the architects of the tumor ecosystem, Cell Stem Cell 24 (2019) 41–53.
[14] M. Luo, M.S. Wicha, Metabolic plasticity of cancer stem cells, Oncotarget 6 (2015) 35141–35142.
[15] A.Z. Ayob, T.S. Ramasamy, Cancer stem cells as key drivers of tumour progression, J. Biomed. Sci. 25 (20) (2018).
[16] J. Hu, Z. Tang, N.M. Beeraka, et al., Multi-pathway therapeutics in colorectal cancer: targeting EMT, CSCs, and non-apoptotic cell death for drug resistance reversal, J. Drug Target. (2025) 1–22.
[17] C. Saygin, D. Matei, R. Majeti, O. Reizes, J.D. Lathia, Targeting cancer stemness in the clinic: from hype to hope, Cell Stem Cell 24 (2019) 25–40.
[18] M. Dean, T. Fojo, S. Bates, Tumour stem cells and drug resistance, Nat. Rev. Cancer 5 (2005) 275–284.
[19] L. Ricci-Vitiani, D.G. Lombardi, E. Pilozzi, et al., Identification and expansion of human colon-cancer-initiating cells, Nature 445 (2007) 111–115.
[20] M. Al-Hajj, M.S. Wicha, A. Benito-Hernandez, S.J. Morrison, M.F. Clarke, Prospective identification of tumorigenic breast cancer cells, Proc. Natl. Acad. Sci. U. S. A. 100 (2003) 3983–3988.
[21] Y.J. Zhu, S.Y. Li, S.S. Yang, Y. Du, Z.Y. Zhang, J.Y. Liu, CD44 on cancer stem cell is a potential immunological and prognostic pan-cancer biomarker, Cancer Cell Int. 25 (2025) 134.
[22] N. Vasan, J. Baselga, D.M. Hyman, A view on drug resistance in cancer, Nature 575 (2019) 299–309.
[23] S.B. Keysar, A. Jimeno, More than markers: biological significance of cancer stem cell-defining molecules, Mol. Cancer Therapeut. 9 (2010) 2450–2457.
[24] C. Zhuang, W. Zhang, C. Sheng, W. Zhang, C. Xing, Z. Miao, Chalcone: a privileged structure in medicinal chemistry, Chem. Rev. 117 (2017) 7762–7810.
[25] Z. Nowakowska, A review of anti-infective and anti-inflammatory chalcones, Eur. J. Med. Chem. 42 (2007) 125–137.
[26] D.I. Batovska, I.T. Todorova, Trends in utilization of the pharmacological potential of chalcones, Curr. Clin. Pharmacol. 5 (2010) 1–29.
[27] S. Ducki, The development of chalcones as promising anticancer agents, Idrugs 10 (2007) 42–46.
[28] J. Yang, J. Lv, S. Cheng, et al., Recent progresses in chalcone derivatives as potential anticancer agents, Anti Cancer Agents Med. Chem. 23 (2023) 1265–1283.
[29] Y. Ouyang, J. Li, X. Chen, X. Fu, S. Sun, Q. Wu, Chalcone derivatives: role in anticancer therapy, Biomolecules 11 (2021).
[30] B. Colmegna, L. Morosi, M. D'Incalci, Molecular and pharmacological mechanisms of drug resistance:an evolving paradigm, Handb. Exp. Pharmacol. 249 (2018) 1–12.
[31] C. Holohan, S. Van Schaeybroeck, D.B. Longley, P.G. Johnston, Cancer drug resistance: an evolving paradigm, Nat. Rev. Cancer 13 (2013) 714–726.
[32] A. Mazurakova, L. Koklesova, D. Vybohova, et al., Therapy-resistant breast cancer in focus: clinically relevant mitigation by flavonoids targeting cancer stem cells, Front. Pharmacol. 14 (2023) 1160068.
[33] O.J. Hussein, D. Elkhalifa, A.F. Hassan, F. Alali, A.E. Al Moustafa, A. Khalil, The role of natural chalcones and their derivatives in targeting prostate cancer: recent updates, Int. J. Mol. Sci. 26 (2025).
[34] R. Michalkova, L. Mirossay, M. Kello, et al., Anticancer potential of natural chalcones: in vitro and in vivo evidence, Int. J. Mol. Sci. 24 (2023).
[35] A. Waterhouse, M. Bertoni, S. Bienert, et al., SWISS-MODEL: homology modelling of protein structures and complexes, Nucleic Acids Res. 46 (2018) W296–W303.
[36] G.M. Morris, R. Huey, W. Lindstrom, et al., AutoDock 4 and AutoDockTools 4: automated docking with selective receptor flexibility, J. Comput. Chem. 30 (2009) 2785–2791.
[37] O. Trott, A.J. Olson, AutoDock vina: improving the speed and accuracy of docking with a new scoring function, efficient optimization, and multithreading, J. Comput. Chem. 31 (2010) 455–461.
[38] B. Schiffrin, S.E. Radford, D.J. Brockwell, A.N. Calabrese, PyXlinkViewer: a flexible tool for visualization of protein chemical crosslinking data within the PyMOL molecular graphics system, Protein Sci. 29 (2020) 1851–1857.
[39] C. Yoon, J. Lu, B.J. Kim, et al., Patient-derived organoids from locally advanced gastric adenocarcinomas can predict resistance to neoadjuvant chemotherapy, J. Gastrointest. Surg. 27 (2023) 666–676.
[40] K. Ganesh, C. Wu, K.P. O'Rourke, et al., A rectal cancer organoid platform to study individual responses to chemoradiation, Nat. Med. (N. Y., NY, U. S.) 25 (2019) 1607–1614.
[41] J. Schindelin, I. Arganda-Carreras, E. Frise, et al., Fiji: an open-source platform for biological-image analysis, Nat. Methods 9 (2012) 676–682.
[42] C.T. Ekanger, M.P. Ramnefjell, M.S.F. Guttormsen, et al., An organoid model for translational cancer research recapitulates histoarchitecture and molecular hallmarks of non-small-cell lung cancer, Cancers (Basel) 17 (2025).
[43] X. Li, M.T. Lewis, J. Huang, et al., Intrinsic resistance of tumorigenic breast cancer cells to chemotherapy, J. Natl. Cancer Inst. 100 (2008) 672–679.
[44] C.A. O'Brien, A. Pollett, S. Gallinger, J.E. Dick, A human Colon cancer cell capable of initiating tumour growth in immunodeficient mice, Nature 445 (2007) 106–110.
[45] S.K. Singh, I.D. Clarke, M. Terasaki, et al., Identification of a cancer stem cell in human brain tumors, Cancer Res. 63 (2003) 5821–5828.
[46] M. Diehn, R.W. Cho, N.A. Lobo, et al., Association of reactive oxygen species levels and radioresistance in cancer stem cells, Nature 458 (2009) 780–783.
[47] F.A. Edalat Haghi, M. Koushkie Jahromi, Exercise as precision medicine: targeting HER2/CD44-Driven therapy resistance in breast cancer (A mini review), Integr. Cancer Ther. 25 (2026) 15347354251407216.
[48] Y. Lee, J.H. Shin, M. Longmire, et al., CD44+ cells in head and neck squamous cell carcinoma suppress T-Cell-Mediated immunity by selective constitutive and inducible expression of PD-L1, Clin. Cancer Res. 22 (2016) 3571–3581.
[49] S. Takaishi, T. Okumura, S. Tu, et al., Identification of gastric cancer stem cells using the cell surface marker CD44, Stem Cell. 27 (2009) 1006–1020.
[50] E.A. Kogan, E.E. Shchelokova, T.A. Demura, et al., [ALDH1, CD133, CD34-positive cancer stem cells in lung adenocarcinoma in patients who had a new coronavirus infection and retained the persistence of viral proteins in the lung tissue], Arkh. Patol. 86 (2024) 5–14.
[51] F. Liu, Y. Qian, The role of CD133 in hepatocellular carcinoma, Cancer Biol. Ther. 22 (2021) 291–300.

[52] Z. Nowakowska, A review of anti-infective and anti-inflammatory chalcones, Eur. J. Med. Chem. 42 (2007) 125–137.
[53] V.R. Yadav, S. Prasad, B. Sung, B.B. Aggarwal, The role of chalcones in suppression of NF-kappaB-mediated inflammation and cancer, Int. Immunopharmacol. 11 (2011) 295–309.
[54] D.I. Batovska, I.T. Todorova, Trends in utilization of the pharmacological potential of chalcones, Curr. Clin. Pharmacol. 5 (2010) 1–29.